RESEARCH



α-Fe₂O₃/ZnO nanocomposite as an efficient photocatalyst for wastewater treatment and flexible electronic device applications

Saisree Sridharan 1 · Sundara Venkatesh Perumalsamy 1 · Jeganathan Kulandaivel 2 · Gopalakrishnan Nammalwar 3 · Hemalatha Parangusan 4 · Deepalekshmi Ponnamma 5

Received: 10 May 2023 / Revised: 8 November 2023 / Accepted: 21 November 2023 / Published online: 7 December 2023 © The Author(s), under exclusive licence to Springer-Verlag GmbH Germany, part of Springer Nature 2023

Abstract

In this work, we report the synthesis of $\alpha\text{-Fe}_2O_3$, ZnO, and $\alpha\text{-Fe}_2O_3$ /ZnO nanomaterials by a simple sol-gel method for photocatalytic dye degradation and flexible electronic applications. X-ray diffraction results reveal that the synthesized samples were rhombohedral and hexagonal wurtzite structures of $\alpha\text{-Fe}_2O_3$, and ZnO nanoparticles, respectively. $\alpha\text{-Fe}_2O_3$ /ZnO composites exhibit the mixed peaks of both $\alpha\text{-Fe}_2O_3$ and ZnO crystal structures which substantiate the formation of $\alpha\text{-Fe}_2O_3$ /ZnO composites. From the optical studies, the band gaps of $\alpha\text{-Fe}_2O_3$, ZnO, and $\alpha\text{-Fe}_2O_3$ /ZnO composites of (1:1) and (1:2) ratios are calculated as 2.11, 3.14, 2.87, and 2.92 eV respectively. Compared to pure $\alpha\text{-Fe}_2O_3$ and pure ZnO nanoparticles, $\alpha\text{-Fe}_2O_3$ /ZnO composites of (1:2) ratio exhibit superior photocatalytic behavior under the irradiation of the natural sunlight and also show good stability for up to five cycles. From the scavenger studies, it is concluded that hydroxyl radicals are the major contributors to the photocatalytic degradation of methylene blue dye molecules. The dielectric behavior of the pure and blended nanoparticles is also investigated in a wide range of frequencies using impedance spectroscopy. The nanoparticles embedded in polyvinyl alcohol (PVA) or $\alpha\text{-Fe}_2O_3$ /ZnO/PVA thin films demonstrate a higher dielectric constant (32.68) and lower loss factor (3.32) than pristine PVA. The AC conductivity (σ_{AC}) of σ -Fe $_2O_3$ /ZnO composites of (1:2) ratio is 10^{-12} S/cm. These findings indicate the possibilities of using σ -Fe $_2O_3$ /ZnO/PVA composites for the fabrication of flexible electronic devices.

Keywords Nanocomposites $\cdot \alpha$ -Fe₂O₃ \cdot Photocatalytic dye degradation \cdot Dielectric studies

- Sundara Venkatesh Perumalsamy srnmcphysics@gmail.com
- Nanomaterials Laboratory, Department of Physics, Sri S. Ramasamy Naidu Memorial College (Affiliated to Madurai Kamaraj University, Madurai – 625 021, Tamil Nadu, India), Sattur, Tamil Nadu 626 203, India
- ² Centre for Nanoscience and Nanotechnology, Department of Physics, Bharathidasan University, Tiruchirappalli, Tamil Nadu 620 024, India
- Department of Physics, National Institute of Technology, Tiruchirappalli, Tamil Nadu 600 015, India
- ⁴ Qatar University Young Scientist Center, Qatar University, P.O. Box 2713, Doha, Qatar
- Materials Science and Technology Program, Department of Mathematics, Statistics and Physics, College of Arts and Science, Qatar University, P. O. Box, 2713 Doha, Qatar

Introduction

In recent times, the environment has been highly polluted due to anthropogenic activities which will bring several serious issues such as climate change, rising sea levels, extreme weather, floods, droughts, and storms [1, 2]. Further, the energy industry and transport sectors emit the majority of greenhouse gases into the atmosphere, and they also play a significant role in environmental pollution. Environmental pollution is a harmful course of action to the soil, landfills in valleys, unprotected aquatic life, and mainly wastewater which flows all around with industrial discharges of dyes, drugs, persistent harmful chemicals, heavy metals, organic pollutants, pesticides, herbicides, phenols, antibiotics, textile effluents, industrial sewage, medical waste, etc. [3]. From the earlier reports, it was found that nearly 100,000 dyes were in usage and 100,000 tons of wastewater in global volume were produced annually from the textile and other industries [4]. Of these, 50% of dyes are only from the textile



industry [5], and the remaining are from tanneries, printing, cosmetic, food, and pharmaceutical industries. These synthetic organic dyes pose a threat to aquatic life disturbing the tropic chain of the ecosystem and causing fatal effects even to human beings [6]. All can be treated with environmentally friendly methods like solvent extraction, coagulation, filtration, membrane separation, advanced oxidation process, ion exchange, and dye degradation [7–9]. Among these methods, solar-driven photocatalytic dye degradation is one of the eco-friendly approaches that will degrade the organic pollutants by oxidation and reduction processes [3]. The survey conducted by the National Centre for Biological Information on the search query from 2007 to 2020 predicted that the pure form of iron oxides played a significant role in the degradation of azo dyes and heavy metals [10]. In recent times, there have been enormous research publications on iron oxides for wastewater treatments. This iron oxide exists in various forms such as α -Fe₂O₃ (hematite), β-Fe₂O₃ (Topotactic phase-instable), α-FeOOH (goethite), δ-FeOOH (feroxyhyte), γ-FeOOH (lepidocrocite), Fe(OH)₃ (iron III oxide hydroxide), γ-Fe₂O₃ (maghemite), and Fe₃O₄ (*magnetite*) [10].

Among the various forms of iron oxides, α -Fe₂O₃ is one of the most stable photocatalysts with high corrosion resistance, high photocatalytic activity, extremely abundant nature, low cost, bio-degradability, and high stability in all kinds of environments, and it was also found that it will play a great role in the research industry [11]. Its band gap value lies in the visible region of the electromagnetic spectrum (2.2–2.4 eV), and hence it can absorb the entire visible light (45%). The photocatalytic property of α -Fe₂O₃ finds application in various energy and environmental crises such as pollution, energy production, energy storage, biological scrutiny on organisms, and pioneering inventions for modern heritage [10]. Therefore, α -Fe₂O₃ is identified as the most suitable material for solar-driven photocatalytic dye degradation and solar-driven photoelectrochemical water-splitting applications. Hence, the researchers have been motivated toward the fabrication of α -Fe₂O₃ nanostructures by various approaches such as sol-gel [12], hydrothermal [13], co-precipitation [14], solvothermal [15], electrochemical deposition of thin films [16], laser-assisted chemical vapor deposition [17], in situ polymerization [18], and also the green synthesis of iron-rich plant productions [19]. Hence, we have adoped a simple sol-gel method for the synthesis of α-Fe₂O₃ nanostructures. However, the photocatalytic dye degradation and water-splitting efficiencies of pure α-Fe₂O₃ nanostructures are very limited and so far from their theoretical value which may be due to the fast recombination rate of photogenerated charge carriers which is hindering their extensive application in photocatalysis [20]. The primary reason is the short lifetime of the photogenerated charge carriers, and not enough diffusion length (2–4 nm) to transfer the hole to the surface of the α -Fe₂O₃ [21]. Numerous attempts have been made to address these limitations, including morphology engineering, element doping, heterostructure formation, overloading of oxygen evolution catalyst, deposition of electrocatalyst, crystal facet engineering, and formation of composites [20].

Among the various attempts, the formation of composites in particular with wide bandgap semiconductors, in particular, TiO₂ [22] and ZnO [23] for the elevation of photocatalytic activities of α-Fe₂O₃ enhances the rate of separation of the photogenerated charge carriers and reduces the photo-corrosive property of α-Fe₂O₃ [24]. Further, the composites make it active in both the visible and UV regions and therefore its photocatalytic efficiency improves under natural sunlight [25–27]. Hence, this work aims the preparation of α -Fe₂O₃, ZnO, and α-Fe₂O₃/ZnO composites and investigates the photocatalytic dye degradation of methylene blue (MB) and dielectric studies. This investigation was on the effects of the integration of α-Fe₂O₃ and ZnO nanomaterials for the ability to offer significant improvements and breakthroughs in the fields of dye degradation and dielectric studies, contributing to sustainable and technologically advanced cost-effective solutions.

Among various combinations, α -Fe₂O₃/ZnO composites of (1:2) ratio exhibit superior photocatalytic activity, and the scavenger analysis reveals that the hydroxyl radicals are the major contributors to the photocatalytic degradation of MB dye molecules. Further, the AC conductivity (σ_{AC}) of α -Fe₂O₃/ZnO composites of (1:2) ratio signifies that it is a suitable candidate for the fabrication of flexible electronic devices at high-frequency ranges also.

Materials and methods

Materials

The analytical grade of iron nitrate nonahydrate (Fe(NO₃)₂·9H₂O), zinc nitrate hexahydrate (Zn (NO₃)₂)·6H₂O, and gelatin ($C_6H_{12}O_6$) were procured from Merck. They were used without further purification.

Synthesis of nanoparticles

Preparation of α-Fe₂O₃

For the evolution of α -Fe₂O₃ nanoparticles (NPs), 0.1 M of iron nitrate and 0.1 M of gelatin were dissolved in double-distilled (DD) water separately and stirred for 30 min. Subsequently, the two precursors were mixed and the final solution was continuously stirred for 3 h along with the heat treatment until it was transformed into a clear solution. After that, the magnetic peddle was removed from the solution, and the heat treatment was continued for the next 3 h. Finally, the dried porous foam-like structures were obtained,



and the product was naturally allowed to cool down for a day. Then, the dried porous form-like structure was ground with the mortar pestle and annealed at 1000 °C for 2 h in the ambient condition. Finally, the reddish brown α -Fe₂O₃ NPs were obtained. The powder samples were finely grained and packed for further studies. The preparation procedure of α -Fe₂O₃ NPs is schematically shown in Fig. 1 a.

Synthesis of ZnO

The precursors of ZnO were prepared by dissolving 0.1 M of zinc nitrate hexahydrate in DD water and the final solution was continuously stirred for 30 min [23]. After that, the same synthesis procedure of α -Fe₂O₃ NPs was adopted to synthesize ZnO NPs. The final white-colored powder was dried, and ground well.

Preparation of α-Fe₂O₃/ZnO nanocomposites

For the preparation of α -Fe₂O₃/ZnO nanocomposites, the prepared α -Fe₂O₃ NPs and ZnO NPs were taken as source

materials. α -Fe₂O₃/ZnO nanocomposites of (1:1) and (1:2) were prepared by using the solid-state reaction technique [21]. In this method, Fe₂O₃ and ZnO NPs were mixed together and ground continuously by using a mortar and pestle for 6 h.

Preparation of films for dielectric studies

0.15 g of α -Fe₂O₃ NPs was dissolved in 5 ml of DD water by ultrasonication. Similarly, 0.15 g of polyvinyl alcohol (PVA) was taken in 2 ml of DD water and heated at 50 °C until the PVA was dissolved. After that, the dissolved NPs were slowly added to the PVA solution and the resultant solution was mixed well overnight (as shown in Fig. 1b). The mixed solution was transferred into a Petri dish and allowed to dry for 3 days in the open-air ambient. Finally, the α -Fe₂O₃/PVA film was fabricated. The above similar procedure was adopted to prepare the ZnO, α -Fe₂O₃/ZnO (1:1), and α -Fe₂O₃/ZnO (1:2) blended with PVA films. The photographs of the prepared films are shown in Fig. 1 c and were used for the dielectric measurements.

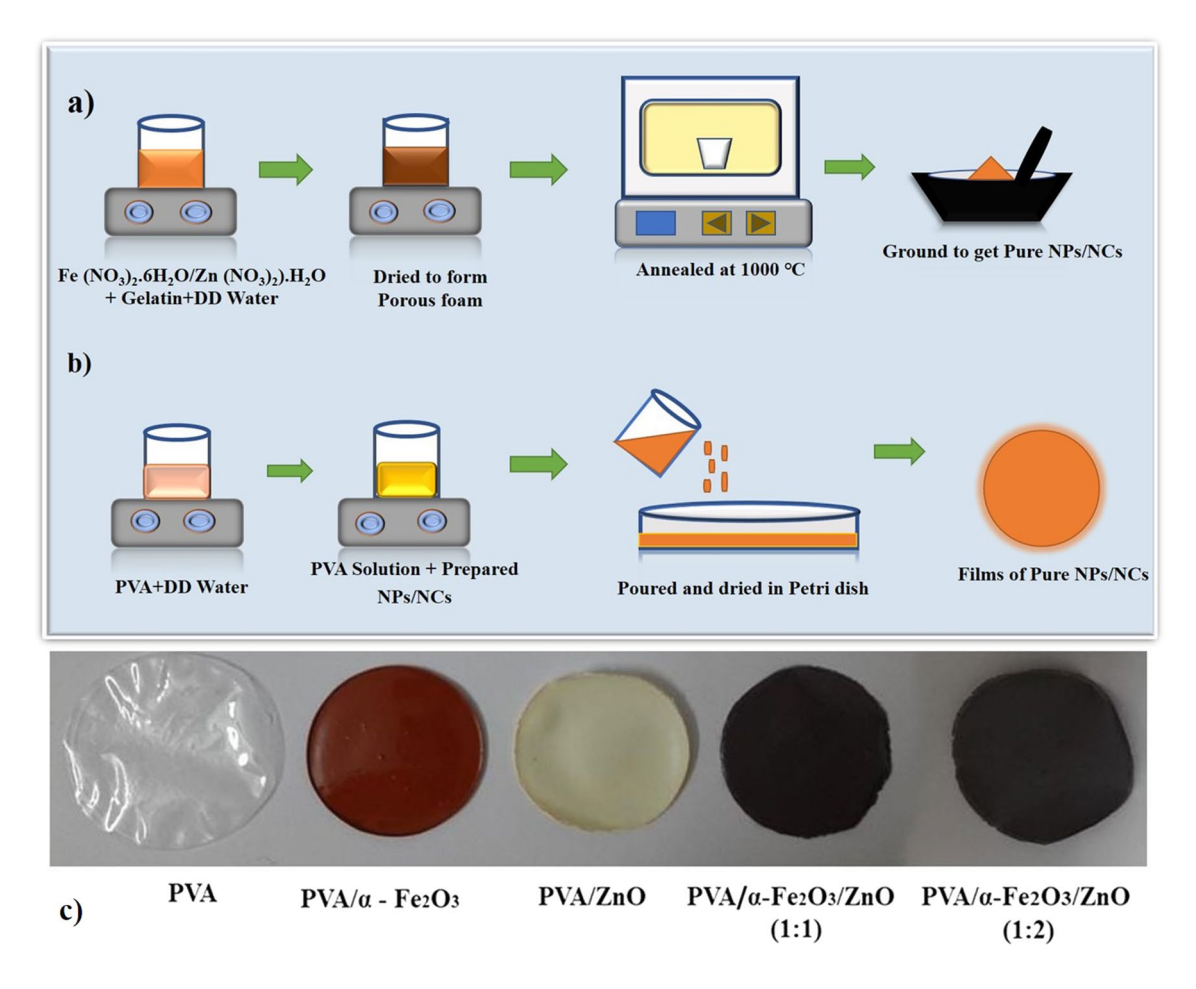


Fig. 1 a, b Schematic representations of NPs and film preparation procedure, and c digital photographs of the prepared pure α -Fe₂O₃, ZnO, and blend composite films, with PVA



Characterization

The structural studies of pure α-Fe₂O₃ NPs, ZnO NPs, and α-Fe₂O₃/ZnO nanocomposites were done by using an X-ray diffractometer (Bruker Eco D8 Advance, Germany) with Cu K_{α} radiation ($\lambda = 1.5406 \text{ Å}$). For the phase identification of the samples, the diffraction patterns were recorded using θ –2 θ geometry between 10 and 80 $^{\circ}$ with a step size of 0.05°. The surface morphologies of the samples were investigated by a field emission scanning electron microscope (Carl Zeiss-Cross Beam 340, Germany). Raman spectra of the samples were recorded in the back-scattering geometry by using Renishaw inVia Raman Spectrometer with an objective lens of 50× magnification. A laser source of 532 nm wavelength was used as an excitation source. In order to cease laser-induced heating in the samples, 1mW laser power was used. Fourier transform infrared (FTIR) spectrum was logged using the Shimadzu IR TRACER-100 FTIR spectrophotometer in the spectral range of 300-4000 cm⁻¹. The photoluminescence studies of the samples were documented by using a HORIBA JOBIN YVON (iHR 550) monochromator. A He-Cd laser of 325 nm wavelength was used as an excitation source. The optical reflectance spectra were evaluated by using the ultraviolet diffuse reflectance spectrophotometer (UV-DRS) (JASCO V-750, Japan). In the dielectric studies, AC conductivity measurements were carried out using a programmable LCR meter (Novocontrol BDS GmbH concept 40, Germany) over the frequency range of 0.01 to $10 \times$ $10^{6} \, \text{Hz}.$

Experimental details of photocatalytic studies

The photocatalytic dye degradation studies of MB dye molecules were undertaken using the prepared nanomaterials as a photocatalyst under natural sunlight at Sattur, Tamil Nadu, India (geographical location: 9.3580 °N, 77.9156°E). For the preparation of the MB dye solution, 10 ppm of MB dye is dissolved in 100 ml of DD water. All the photocatalytic experiments were conducted using 0.15 g of photocatalyst (α -Fe₂O₃, ZnO, α -Fe₂O₃/ZnO (1:1), and α -Fe₂O₃/ZnO (1:2)) in 10 ppm of MB dye solution. In order to attain the complete dispersion of the catalyst, the above-prepared colloidal solution was sonicated, and the solution was kept under natural sunlight on a sunny day. Under illumination, the degradation was observed in the solution. To examine the degradation of MB dye molecules, 5 ml of dye solution was collected at a regular time interval of 15 min from 0 to 75 min. Finally, the collected solutions were filtrated, and the UV-Vis absorption spectra were documented by using the UV-visible spectrophotometer (JASCO V-750).



Radical trapping analysis

To establish the degradation mechanism of MB dye using the prepared samples, the radical trapping analysis was carried out using $\alpha\text{-Fe}_2O_3/ZnO$ (1:2) nanocomposites. For this study, benzoquinone (BQ), isopropanol (IPA), and ethylenediaminetetraacetic acid (EDTA) were taken as scavengers for superoxide radicals, hydroxyl radicals, and holes respectively. To examine the photo-corrosion and photostability of the $\alpha\text{-Fe}_2O_3/ZnO$ (1:2) composites, the photocatalytic degradation of MB dye molecules was repeated for up to 5 cycles under the illumination of natural sunlight.

Results and discussion

Structural and optical properties of α-Fe₂O₃/ZnO nanocomposites

Fig. 2 a depicts the XRD patterns of α -Fe₂O₃ NPs, ZnO NPs, α -Fe₂O₃/ZnO (1:1), and α -Fe₂O₃/ZnO (1:2) nanocomposites. All the reflections observed in the XRD spectrum of pure α -Fe₂O₃ NPs are in concurrence with the JCPDS Card No. 00-033-0664 and correspond to the Rhombohedral structure [28]. For the ZnO NPs, the observed XRD peaks are in concurrence with the JCPDS Card. No. 01-036-1451, and corresponds to the hexagonal wurtzite structure with P63 mc space group [29]. In the XRD spectra of α -Fe₂O₃/ZnO nanocomposites, all the reflections correspond to the peaks of ZnO and α -Fe₂O₃ NPs. This evidences the formation of α -Fe₂O₃/ZnO nanocomposites and the absence of secondary peaks shows the sample is free from impurities.

The mean crystalline size and strain of the synthesized NPs and their composites are found by the Williamson-Hall (W-H) equation.

$$\beta_{hkl}\cos\theta = \frac{k\lambda}{D} + 4\varepsilon\sin\theta\tag{1}$$

where D is the crystalline size of the NPs, k is the shaping factor or Scherrer constant, λ is the wavelength of the X-ray used, β is the value of full-width at half maximum (FWHM) of the diffraction peak, and θ represents the Bragg angle, and ϵ is the microstrain [30]. The mean crystalline size of pure α -Fe₂O₃ and ZnO NPs is calculated as 50 and 27 nm, respectively. For the composite samples, the mean crystalline size is 23 and 20 nm for the 1:1 and 1:2 ratios, respectively. The variation of the crystalline size and strain are depicted in Fig. 2 b.

The FTIR spectra of α -Fe₂O₃, ZnO, and α -Fe₂O₃/ZnO (1:1), (1:2) composites are shown in Fig. 3 a. In the FTIR spectrum of α -Fe₂O₃ NPs, the wavenumbers at 451 and 566 cm⁻¹ signify the Fe–O stretching, and bending modes, respectively [31], whereas, in ZnO, the small transmission

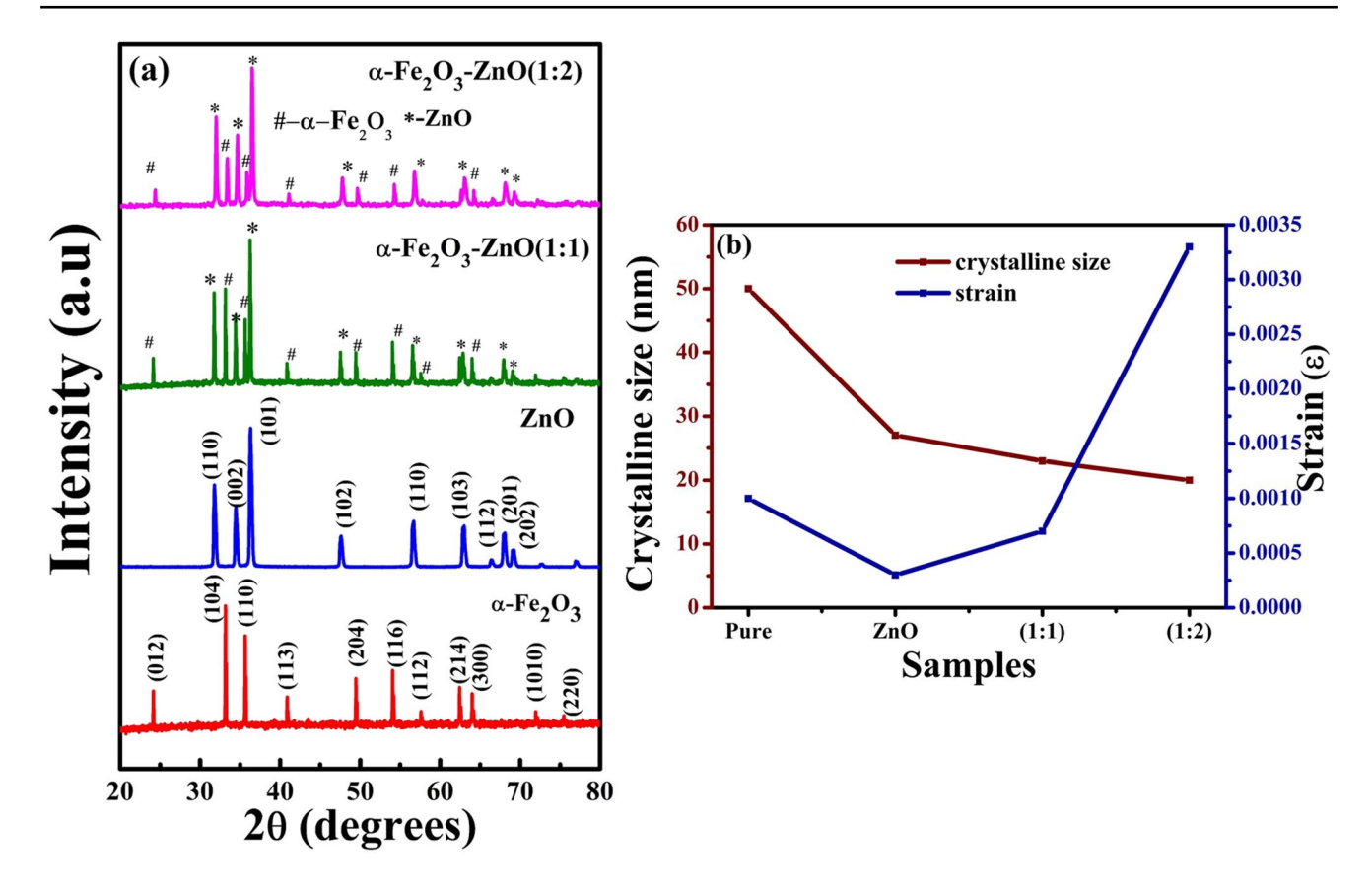
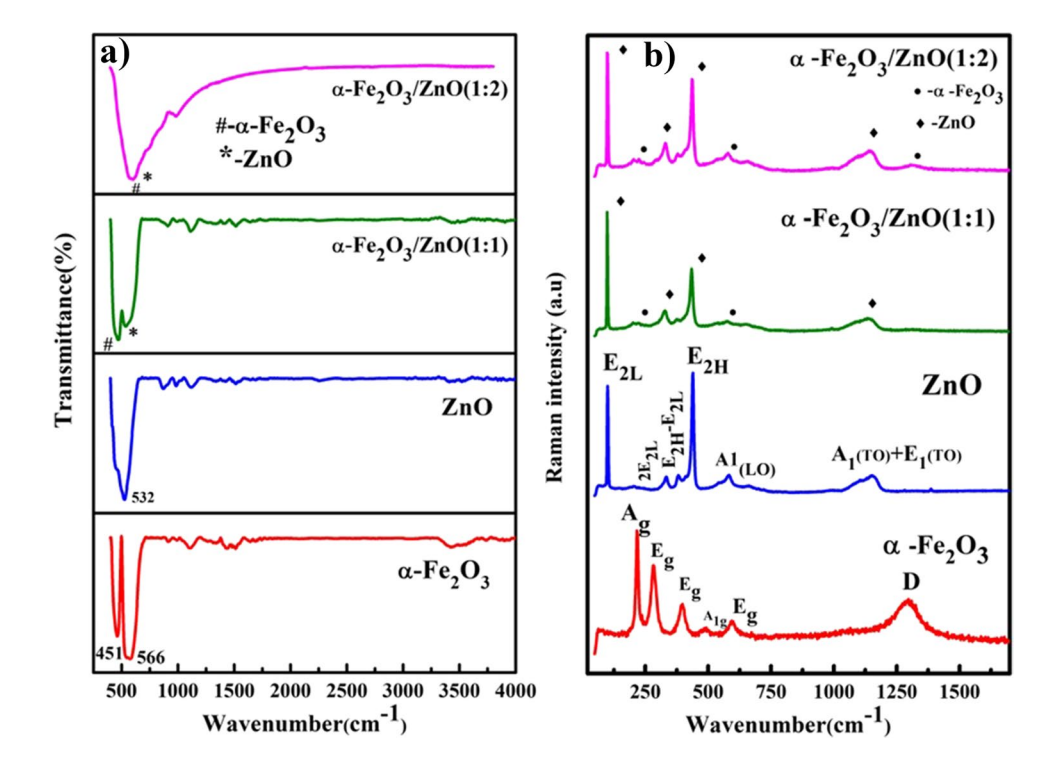


Fig. 2 a XRD patterns of α -Fe₂O₃/ZnO (1:1), and α -Fe₂O₃/ZnO (1:2) nanocomposites, and **b** variation of crystalline size and strain for pure and composite samples

Fig. 3 a FTIR spectra and b Raman spectra of α -Fe₂O₃, ZnO, and their composites





peak at 440 cm $^{-1}$ is merged with the peak at 532 cm $^{-1}$ which is due to the Zn–O stretching mode [32]. In the composite samples of (1:1) and (1:2), the combined peaks of Fe $_2$ O $_3$ and ZnO NPs are observed along with small peaks at 913 cm $^{-1}$ representing amines, 1424 cm $^{-1}$ for –COOH symmetric stretch, 1532 cm $^{-1}$ shows N–H bending vibration, 1630 cm $^{-1}$ for C=O stretch, and 3433 cm $^{-1}$ for O–H stretch respectively [33]. These peaks may be ascribed to the addition of gelatin in the preparation process.

Fig. 3 b shows the Raman spectra of α -Fe₂O₃, ZnO, and their nanocomposites. It is a basic technique to examine the vibrational symmetry of molecules. α -Fe₂O₃ belongs to the D_{3d}^{6} space group and possesses seven typical Raman active modes, namely two A_{1g} modes and five E_{g} modes [34]. In the Raman spectrum of α -Fe₂O₃ NPs, the peaks observed at 220 and 493 cm⁻¹ belong to the A_{g} and the peaks observed at 288, 409, and 604 cm⁻¹ agree with E_{g} symmetry. D state of sp3 carbon atoms observed at 1297 cm⁻¹ corresponding to the two magnon scattering modes corroborates with the XRD results of rhombohedral structure. In the Raman spectrum of ZnO NPs, the peaks observed at 99.3, 199, 335.9, and 435.6 cm⁻¹ correspond to the E₂ low, 2E₂ low, E₂ high-E₂ low, and E₂ high phonon modes, respectively [35]. In addition to this, the peaks observed at 588 and 1155 cm⁻¹ belong to

the $A_1(LO)$ and $A_1(TO)+E_1(TO)$, respectively [36]. This observed result substantiates the wurtzite crystal structure of ZnO NPs. The Raman spectra of composite samples confirm the formation of α -Fe₂O₃/ZnO composites and its intensity differs with respect to the ratios of α -Fe₂O₃ and ZnO.

Fig. 4 shows the FESEM images of pure α -Fe₂O₃, ZnO, and their nanocomposites. The particle size of α -Fe₂O₃, ZnO, and their composites have been calculated using Image J software and are pictured in Fig. 5. The particle sizes of the α -Fe₂O₃ and ZnO NPs are 460 and 481 nm respectively. From the particle size measurements, it is noticed that the particles are too big which is attributed to the agglomeration particles due to the post-annealing process at a very high temperature of 1000 °C. This agglomeration of particles happens due to the electrostatic nature and van der Waals forces on high-temperature annealing [37]. This high-temperature annealing is unavoidable in the formation of α-Fe₂O₃ since only 1000 °C and above postannealing temperature ensures the formation of α-Fe₂O₃ in pure form. The particle size of the composite samples (1:1) and (1:2) ratio is in the order of 529 and 484 nm respectively.

Figure 6(a) illustrates the photoluminescence spectra of the pure α -Fe₂O₃ NPs, pure ZnO NPs, and α -Fe₂O₃/ZnO

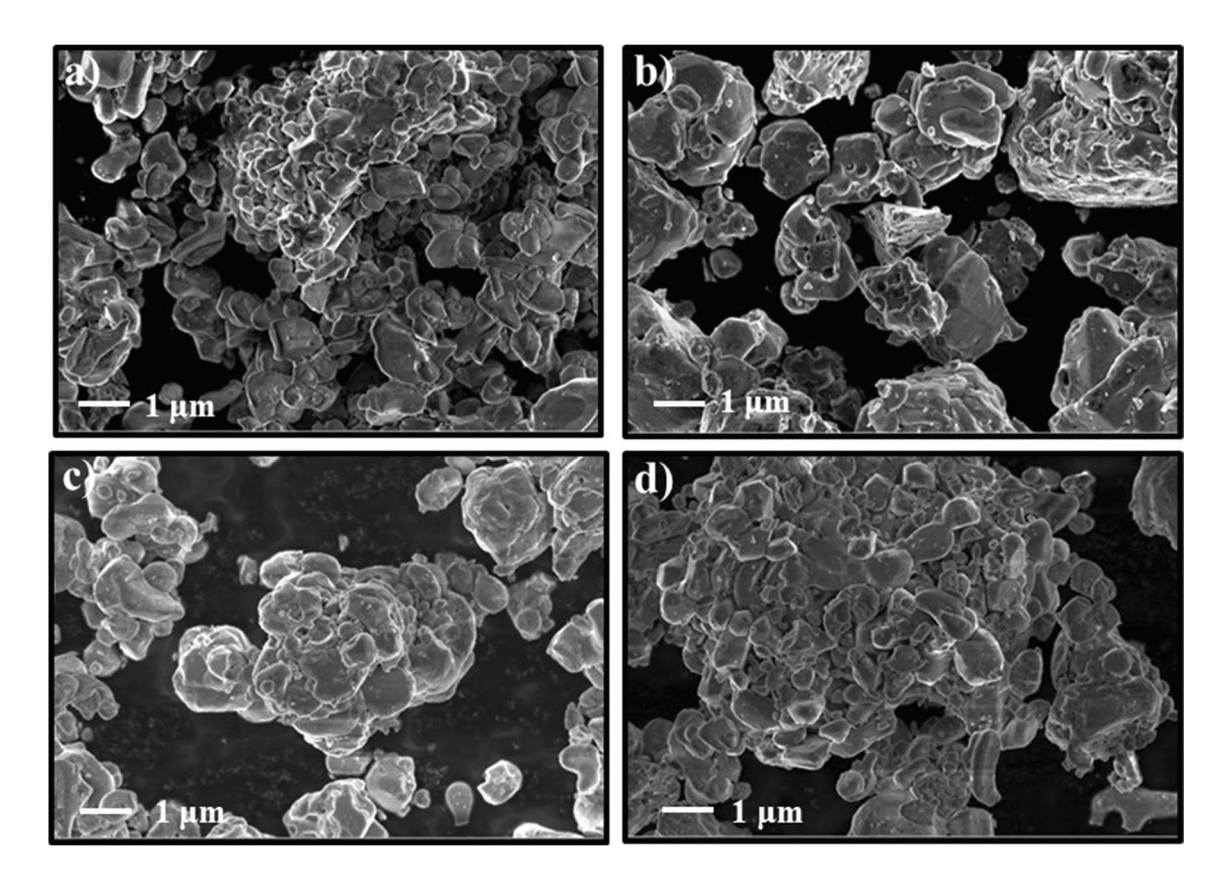


Fig. 4 FESEM images of a α -Fe₂O₃, b ZnO, c α -Fe₂O₃/ZnO (1:1) composite, and d α -Fe₂O₃/ZnO (1:2) composite



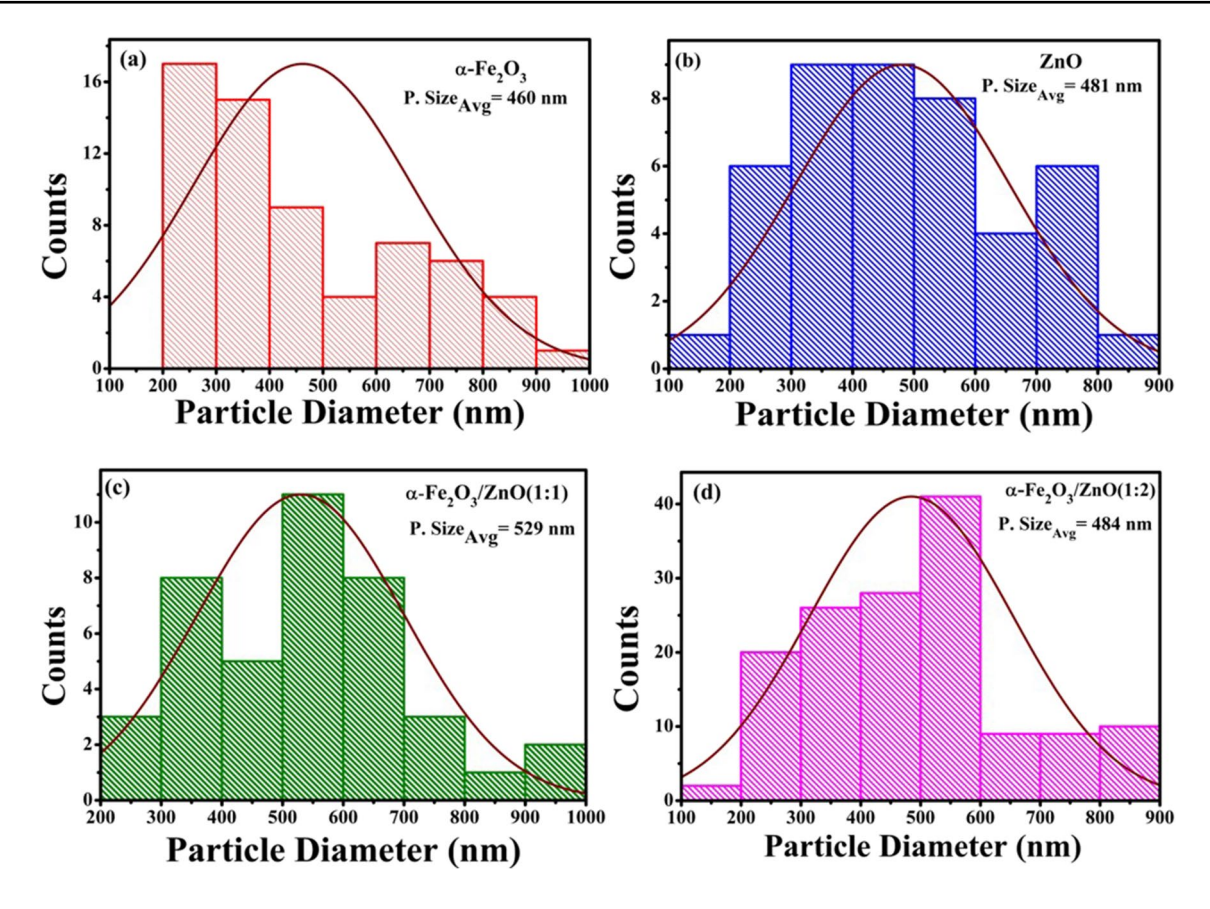


Fig. 5 Particle size distribution of a α -Fe₂O₃, b ZnO, c α -Fe₂O₃/ZnO (1:1), and d α -Fe₂O₃/ZnO (1:2) composites

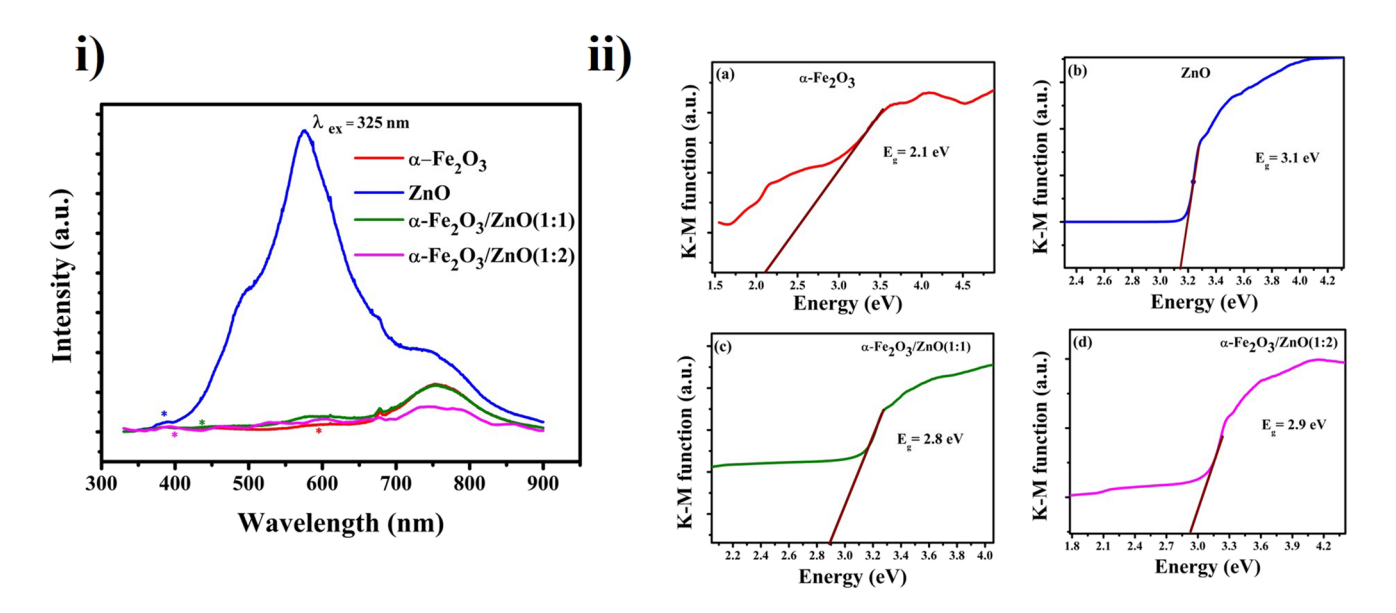


Fig. 6 (i) Photoluminescence spectra of α-Fe₂O₃, ZnO, α-Fe₂O₃/ZnO (1:1), and α-Fe₂O₃/ZnO (1:2) nanocomposites and (ii) UV-diffuse reflectance spectroscopy spectra of (a) α-Fe₂O₃, (b) ZnO, (c) α-Fe₂O₃/ZnO (1:1), and (d) α-Fe₂O₃/ZnO (1:2) nanocomposites



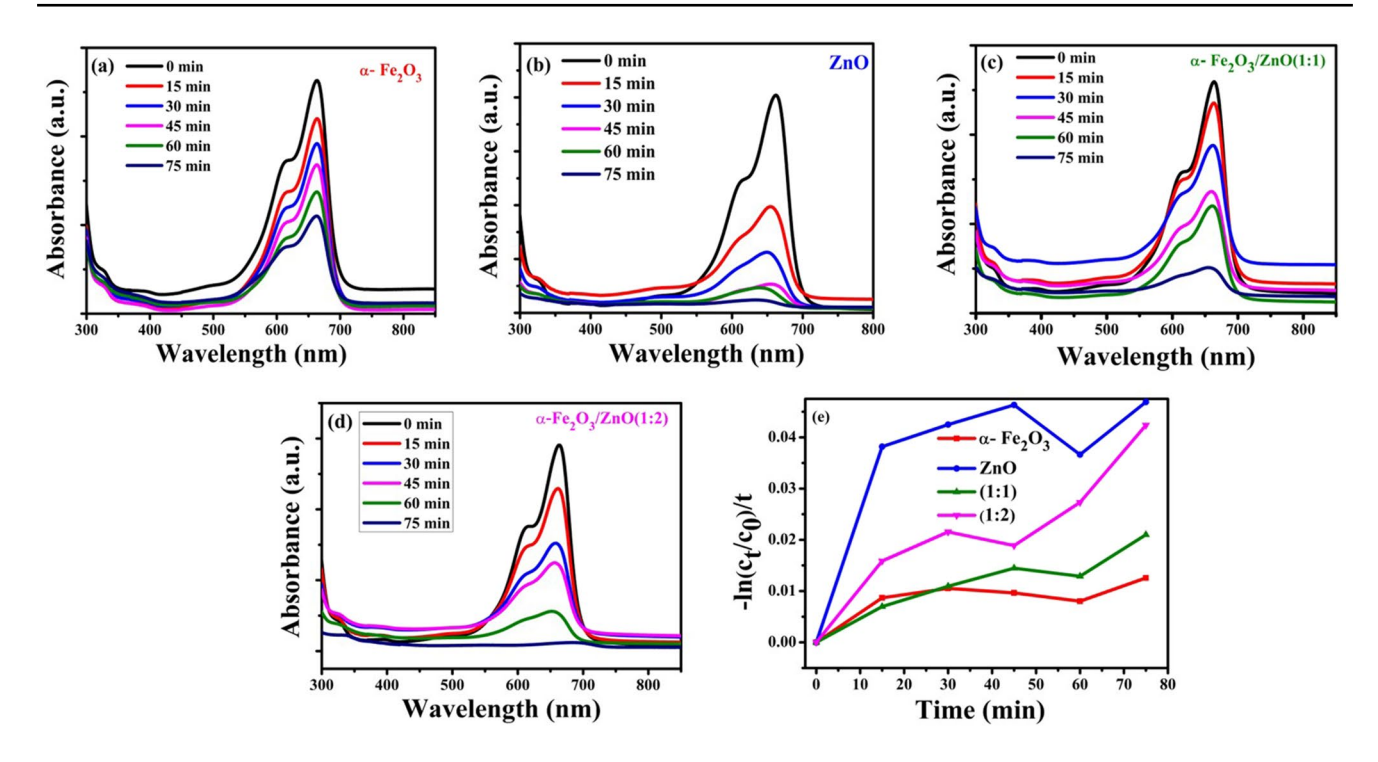


Fig. 7 Dye degradation studies of $\bf a$ α -Fe₂O₃, $\bf b$ ZnO, $\bf c$ α -Fe₂O₃/ZnO (1:1), $\bf d$ α -Fe₂O₃/ZnO (1:2) nanocomposites, and $\bf e$ degradation kinetics of the samples

nanocomposites. In the photoluminescence spectrum of pure α-Fe₂O₃ NPs, the observed emission peak at around 595 nm corresponds to the band edge emission of α -Fe₂O₃ [38]. Similarly, the UV emission peak observed at 386 nm in the ZnO NPs is due to its near band edge emission [39]. In addition to this, the dominant and broad emission peaks observed at 469 and 577 nm confirm the presence of oxygen vacancies in the ZnO NPs [40]. In the case of (1:1) α-Fe₂O₃-ZnO nanocomposite, the band edge emission is observed at 579 nm. Further increasing the composition of ZnO to attain the (1:2) α -Fe₂O₃-ZnO nanocomposite, the band edge emission is observed at 436 nm which represents the blue shift of the band edge emission. From the observation of composite samples, it is noticed that the energy gap of the composites increases from the pure α -Fe₂O₃ NPs when increasing the composition of ZnO. Furthermore, the defect-mediated emission is suppressed in the composite samples. Apart from this, the broad peak observed at 755 nm corresponds to the glass substrate since all the powder samples are fixed in glass substrates in order to record the photoluminescence spectra. It corroborates with the earlier report [41].

Figure 6(b) depicts the Kubelka-Munk (K-M) function vs. energy plot of the pure α -Fe₂O₃ NPs, pure ZnO NPs, and α -Fe₂O₃/ZnO nanocomposites. The K-M function is calculated by using the following equation.



where R is the reflectance data concerning the wavelength. The band gap of α -Fe₂O₃ and ZnO NPs is found to be 2.11 and 3.14 eV, respectively. Similarly, the energy gap of α -Fe₂O₃-ZnO nanocomposites of (1:1) and (1:2) ratio is calculated as 2.87 and 2.92 eV, respectively. From this, it is observed that the band gap value obtained from PL spectra is endorsed by the UV-DRS spectra.

The Urbach energy is calculated using the reflectance data from Eqs. 3 and 4:

$$\alpha = \alpha_0 \exp\left(\frac{hv}{E_u}\right) \tag{3}$$

$$\ln\left(F(R)\right) = \ln\beta + \frac{h\nu}{E_u} \tag{4}$$

where $\alpha = \text{Ln}(F(R))$, $\beta = 2\alpha_0/S$ (Scattering coefficient) is a constant, h is the Planck constant, ν is frequency, and E_u is the Urbach energy [42].

The Urbach energy for α -Fe₂O₃ is 0.963 meV, and ZnO is 1.110 meV. For the composite samples, α -Fe₂O₃/ZnO (1:1) is 1.932 meV, and (1:2) sample is 1.388 meV calculated from Eq. 4. From the Urbach energy, it is clearly known



 Table 1
 Pseudo-first-order
 kinetics
 value
 of
 prepared
 composites

 with their percentage of degradation

Sample	Percentage of degradation (%)	Rate constant K (min ⁻¹)
α-Fe ₂ O ₃	60	0.0086
ZnO	94	0.0421
α -Fe ₂ O ₃ /ZnO (1:1)	80	0.0132
α -Fe ₂ O ₃ /ZnO (1:2)	96	0.0251

that the molecules α -Fe₂O₃/ZnO (1:1) and (1:2) samples are highly disordered caused by agglomeration [25].

Photocatalytic dye degradation α -Fe $_2$ O $_3$ /ZnO nanocomposites

The photocatalytic dye degradation performance of pure Fe₂O₃, pure ZnO, and their composites was investigated by using MB dye molecules under natural sunlight. Fig. 7 a-d depict the time-dependent UV-Vis absorption spectra for the photocatalytic degradation of MB dye molecules using pure α -Fe₂O₃, pure ZnO, and their composites respectively. So far, the previous reports have achieved the degradation of MB to 120 min under solar irradiation [23], and a new improvement has been made. From the absorption spectra of all the samples, it is noticed that the intensity of the characteristic peak of the MB dye molecule (~664 nm) quenches concerning the irradiation time of the sunlight. The percentage of degradation of the dye molecules for all four samples is represented in Table 1. The results show that the (1:2) ratio of α-Fe₂O₃-ZnO nanocomposite exhibits superior photocatalytic dye degradation performance of 96% within 75 min. The sample's degradation efficiency is found using Beer Lambert's law (Eq. 5).

Percentage of Degradation(%) =
$$\left(1 + \frac{C_t}{C_0}\right) \times 100$$
 (5)

where C_0 is the dye molecules' concentration at t = 0 min and C_t is the dye molecules' concentration concerning irradiation time t. The pseudo-first-order kinetic ratio (K) is quantified using the given relation (Eq. 6) and its values are tabulated in Table 1. Further, the variation of the pseudo-first-order kinetic ratio for all the samples is depicted in Fig. 7 e.

$$\ln\left(\frac{C_t}{C_0}\right) = Kt \tag{6}$$

The pseudo-first-order rate of Fe_2O_3 -ZnO composite (1:2) is found to be $0.0251~\text{min}^{-1}$. The degradation rate constant for α -Fe $_2O_3$ is very low and for ZnO is high. Thus, the composites is formed to improve the degradation of α -Fe $_2O_3$ with the help of ZnO and consequently, the degradation rate of the composite also increases as the ratio of ZnO increases.

From the comparison as shown in Table 2, all the above nanocomposites degrade MB dye molecules at various time intervals, and α -Fe₂O₃/ZnO nanocomposite degrades the MB dye molecules at a faster rate, proving that it is a suitable candidate for the dye degradation of MB dye molecules.

Degradation mechanism with cyclic stability

With the following equations, the dye degradation mechanism of MB dye molecules using α -Fe₂O₃/ZnO nanocomposite is explained in detail.

Table 2 Comparison of MB dye molecules' degradation efficiency with various photocatalysts

Photocatalyst	Light source	Degradation time (min)	Degradation efficiency (%)	Reference
α-Fe ₂ O ₃	Sunlight	90	96	[43]
ZnO/mesoporous silica (GSBA-15)	Sunlight	90	94.9	[44]
α-Fe ₂ O ₃ /ZnO	Sunlight	120	95	[23]
α-Fe ₂ O ₃ /ZnO	Tungsten lamp (40W)	45	65	[21]
Fe ₃ O ₄ /ZnO	Sunlight	120	88	[45]
rGO/Fe ₃ O ₄ -TiO ₂	Sunlight	55	99	[46]
rGO/TiO ₂	Sunlight	30	91	[47]
WO ₃ /ZnO/rGO	Sunlight	90	94	[48]
V ₂ O ₅ /CeO ₂	Halogen lamp (150W)	25	98	[49]
ZnO/ZnCr ₂ O ₄	UV-light	120	93	[50]
α -Fe ₂ O ₃ /ZnO	Sunlight	75	96	Present work



$$\alpha - Fe_2O_3/ZnO + hv (Photons)$$

$$\rightarrow \alpha - Fe_2O_3/ZnO(e^- CB)$$

$$+\alpha - Fe_2O_3/ZnO (h^+ VB)$$
(7)

$$\alpha - Fe_2O_3/ZnO(e^- CB) + O_2 \rightarrow \alpha - Fe_2O_3/ZnO + O^{2-}$$
(8)

$$\alpha - Fe_2O_3/ZnO\left(h^+\ VB\right) + H_2O \rightarrow \alpha - Fe_2O_3/ZnO + OH^+ + h^+$$
 (9)

$$OH^+ + MB \ dye \rightarrow \deg \ raded \ products \ (H_2O, CO_2, etc.)$$
(10)

This is the electrons and hole transfer mechanism for the Z scheme heterojunction (α -Fe₂O₃ and ZnO), bare Fe₂O₃, and ZnO. Transferring electrons from the conduction band (CB) of α -Fe₂O₃ to the valance band (VB) of ZnO generates more reactive oxygen species for the degradation of organic dye molecules [23].

The stability study of the photocatalyst is the key decisive parameter for the selection of the potential catalyst for the photocatalytic degradation process. Fig. 8 a shows the recycling study of $\alpha\text{-Fe}_2\text{O}_3\text{-ZnO}$ nanocomposite (1:2). For the recycle studies, $\alpha\text{-Fe}_2\text{O}_3\text{-ZnO}$ nanocomposite (1:2) was taken as a photocatalyst. After the successful completion of the degradation process, the catalyst was retrieved from the dye solution. The retrieved catalyst was taken into a new dye solution, and the degradation process was repeated for up to 5 cycles. From the repeatability studies, it is ascertained that the photocatalytic degradation efficiency is nominally decreased from 96.7 (first cycle) to 90% (fifth cycle). This result ascertains that $\alpha\text{-Fe}_2\text{O}_3\text{-ZnO}$ nanocomposite (1:2) is having appreciable photostability.

Usually, the dye degradation will take place due to the photo-generated charge carriers (electrons and holes) and other highly reactive radicals such as O_2^{--} , OH, and HO_2^{--} . From the observation, it is perceived that the α -Fe₂O₃/ZnO nanocomposite (1:2) has acted as a feasible photocatalyst for the degradation of MB dye molecules. In order to understand the phenomenon of photodegradation, the

radical trapping test was investigated for α -Fe₂O₃/ZnO nanocomposite (1:2) and is shown in Fig. 8 b. This result shows lesser degradation for IPA-added dye solution. This evidences that the hydroxyl radicals play a vital role in the photocatalytic degradation process of MB dye molecules [51]. In addition to this, the holes and superoxide radicals also contribute to the photocatalytic dye degradation process of MB dye molecules. However, their contribution is small compared to the hydroxyl radicals. From the scavenger studies, it is concluded that hydroxyl radicals are the primary contributor to the photocatalytic degradation of MB dye molecules.

Dielectric studies of α-Fe₂O₃/ZnO nanocomposites

In the current work, the dielectric properties of a composite consisting of /Fe₂O₃/ZnO/PVA were examined in order to determine whether it would be feasible to use it for energy storage applications. At room temperature, dielectric studies were taken in Broadband Dielectric Spectroscopy (BDS). The calculated values are from the principles of dielectric studies [52–54] of polymer materials in high-frequency ranges (mHz-GHz) observed in BDS. Bulk material aligns the charges of the material in fields making the overall polarization to find the dielectric constant, dielectric loss, and AC conductivity (σ_{ac}).

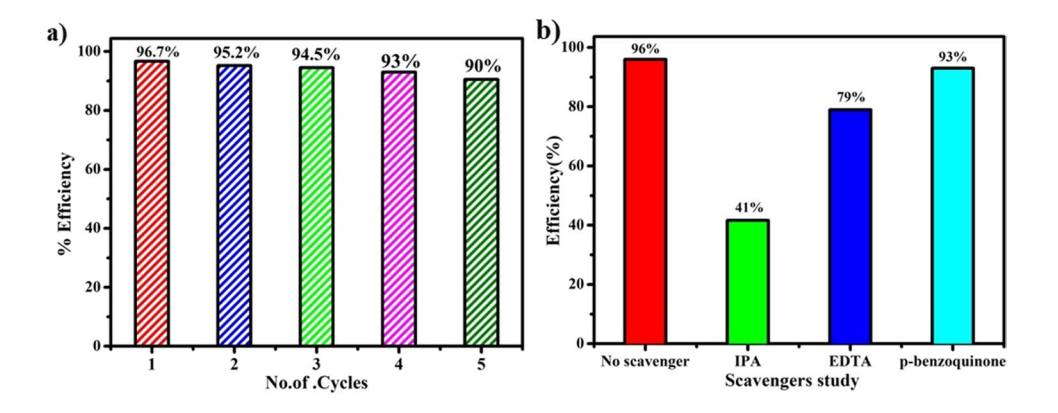
$$\varepsilon_r = \varepsilon' + i\varepsilon'' \tag{11}$$

$$\tan \delta = \frac{\varepsilon''}{\varepsilon'} \tag{12}$$

$$\sigma_{AC} = \omega \varepsilon_0 \varepsilon_r \tan \delta \tag{13}$$

where ε_r is the dielectric constant of the bulk material, ε_0 is the relative permittivity (8.854×10⁻¹² F/m), ε' is the real dielectric part, ε'' is the imaginary dielectric part, $\tan\delta$ is the tangent loss of the dielectric material, ω is the frequency in Hz, and σ_{AC} is the AC conductivity of the polymer dielectric material. The real part of dielectric permittivity is the dielectric

Fig. 8 a Photocatalytic stability, and **b** radical trapping test of α-Fe₂O₃/ZnO nanocomposite (1:2)





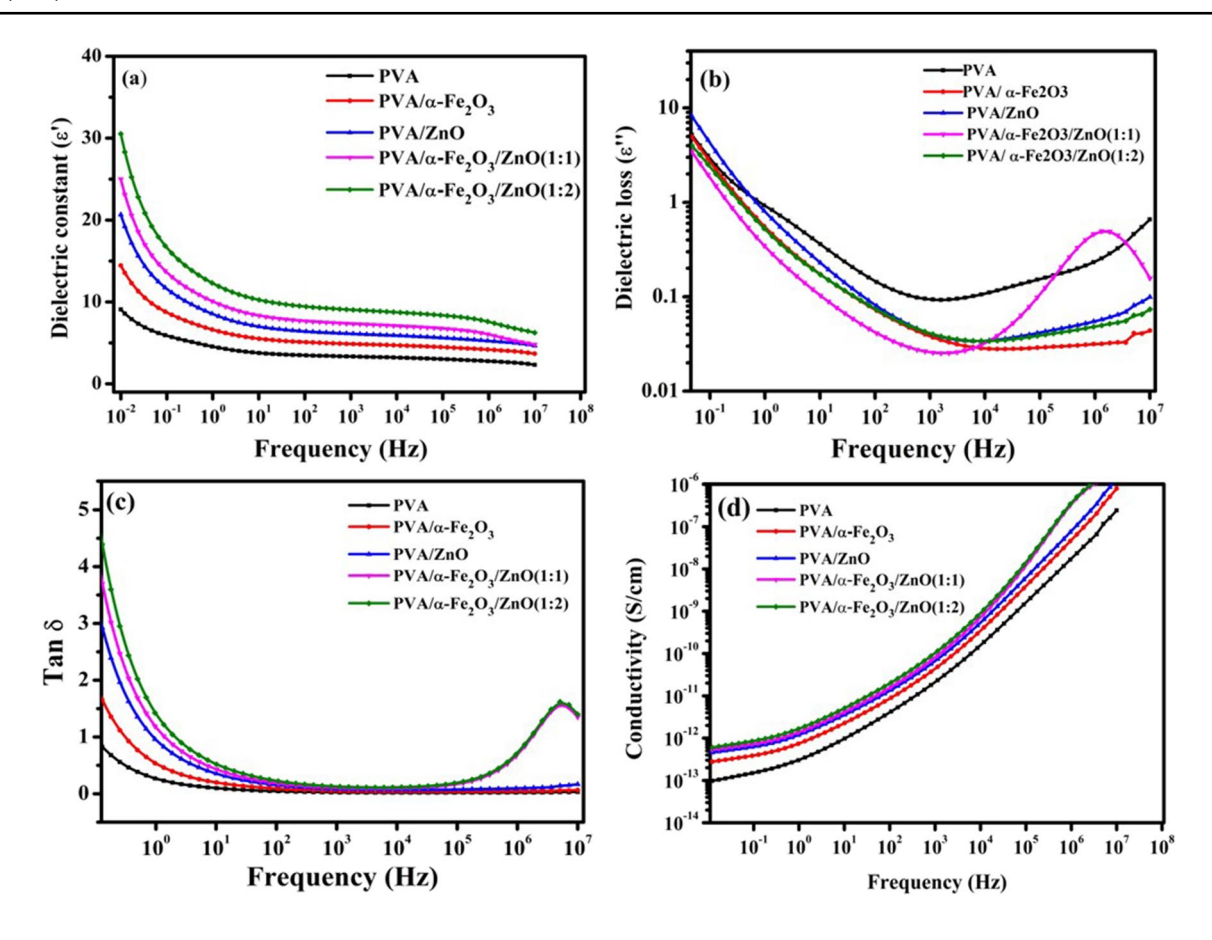


Fig. 9 Graphical representation of dielectric properties of polymer-bound α -Fe₂O₃ and its composites. a Real part of dielectric constant (ε'), b imaginary part of dielectric loss (ε"), c variation of dielectric loss (δ), and d AC conductivity (σ_{AC})

constant of the materials and the imaginary part of permittivity explains the dielectric loss from the tangent loss of dielectric material at room temperature (Fig. 9). The prepared films α-Fe₂O₃/PVA and ZnO/PVA show interfacial polarization of the dipoles at the input frequency [55]. The α -Fe₂O₂/ZnO/PVA (1:1) ratio film exhibits instability as the dielectric constant value drops out to zero at a high frequency losing its polarizability (Fig. 9a). Therefore, the sample α -Fe₂O₃/ZnO/PVA (1:2) stands for application purposes. The dielectric constant of α -Fe₂O₃/ZnO/PVA (1:2) film is 32.68 calculated from Eq. 11. And also, the dielectric loss of the α -Fe₂O₃/ZnO/PVA (1:2) film is very low (3.32) from Eq. 12 compared with the other samples. The difference in the dielectric constant concerning frequency shows that the dielectric constant rises at lower frequencies and falls at higher frequencies as shown in Fig. 9 a. This increased dielectric constant is due to Maxwell-Wagner polarization, which is primarily produced by conductor-insulator interactions. Furthermore, this interfacial polarization is caused by the accumulation of space charge polarization at the interfaces. The σ (AC) conductivity of the α -Fe₂O₃/ZnO/ PVA (1:1) is high (10^{-12}) as shown in Fig. 9 d. In all films, the conductivity increases with frequency. The dielectric loss factor is a standard definition of power outage in a dielectric

medium (tan δ). The frequency evolution of the dielectric loss factor for all films is shown in Fig. 9 c. Tangent loss decreases as frequency increases, as seen in Fig. 9 c.

Conclusion

The sol-gel route of gelatin-mediated α -Fe₂O₃ and their composites were successfully synthesized for the applications of wastewater treatment and flexible electronic devices. XRD results revealed the rhombohedral structure for α-Fe₂O₃ and the hexagonal structure for ZnO and evidence of the formation of their composites. Raman studies confess both Ag and Eg symmetry for α-Fe₂O₃ and substantiate the XRD results. The UV-DRS investigations have yielded valuable insights into the band gap values of various materials. Specifically, α-Fe₂O₃, ZnO, and α -Fe₂O₃/ZnO composites with (1:1) and (1:2) ratios have demonstrated band gap values of 2.11, 3.14, 2.87, and 2.92 eV, respectively. Among these, the α-Fe₂O₃/ZnO composite with a (1:2) ratio stands out for its superior photocatalytic performance when exposed to natural sunlight. Furthermore, it exhibits remarkable stability over five cycles



of use. Scavenger studies have led to the conclusion that hydroxyl radicals play a pivotal role in the photocatalytic degradation of MB dye molecules. $\alpha\text{-Fe}_2\text{O}_3/\text{ZnO/PVA}$ thin films demonstrate a higher dielectric constant (32.68) and lower loss factor (3.32) than pristine PVA. The AC conductivity (σ_{AC}) of $\alpha\text{-Fe}_2\text{O}_3/\text{ZnO}$ composites of (1:2) ratio is 10^{-12} S/cm. All of the experimental results suggest that $\alpha\text{-Fe}_2\text{O}_3/\text{ZnO}$ (1:2) sample can be utilized as a promising candidate for the photocatalytic degradation of dye and flexible electronic devices. The novelty of this work is the multifunctionality opening up a new way of research to integrated and efficient devices. These environmentally friendly materials are desirable, sustainable, and costeffective for production in large quantities.

Acknowledgements SS and PSV would like to thank Dr. S. Amirthapandian, Materials Science Group and Homi Bhabha National Institute, Indira Gandhi Center for Atomic Research, Kalpakkam-603102, Tamil Nadu, India, for extending FESEM and Raman studies. PSV also would like to acknowledge the Department of Biotechnology, Ministry of Science and Technology, Govt. of India, New Delhi, for the financial support under the STAR College Scheme (HRD-11011/48/2021-HRD-DBT).

Author contribution Saisree Sridharan: conceptualization, methodology, formal analysis, investigation, and writing. Sundara Venkatesh Perumalsamy: conceptualization, investigation, review and editing, supervision, and funding acquisition. Jeganathan Kulandaivel, Gopalakrishnan Nammalwar, Hemalatha Parangusan, and Deepalekshmi Ponnamma: resources and review and editing.

Funding This study received financial support from the Department of Biotechnology, Ministry of Science and Technology, Govt. of India, New Delhi, under the STAR College Scheme (HRD-11011/48/2021-HRD-DBT).

Data availability The data that support the findings of this study are available from the corresponding author upon reasonable request.

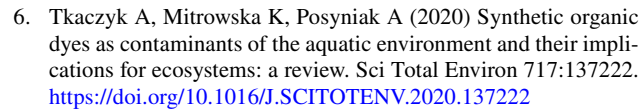
Declarations

Ethical approval Not applicable.

Competing interests The authors declare no competing interests.

References

- Dael S, Sporer M, Tomescu M (2020) Tracking progress towards Europe's climate and energy targets
- Füssel H-M Climate change, impacts and vulnerability in Europe 2012 (EEA Report No 12/2012) - Version of 20.06.2013
- Saravanan A, Kumar PS, Vo DVN et al (2021) Photocatalysis for removal of environmental pollutants and fuel production: a review. Environ Chem Lett 19:441–463
- Ali H (2010) Biodegradation of synthetic dyes a review. Water Air Soil Pollut 213:251–273
- Arora S (2014) Textile dyes: it's impact on environment and its treatment. J Bioremed Biodegr 05. https://doi.org/10.4172/2155-6199.1000e146



- Hitam CNC, Jalil AA (2020) A review on exploration of Fe2O3 photocatalyst towards degradation of dyes and organic contaminants. J Environ Manage 258. https://doi.org/10.1016/j.jenvman.2019.110050
- Ganeshbabu M, Kannan N, Venkatesh PS et al (2020) Synthesis and characterization of BiVO4nanoparticles for environmental applications. RSC Adv 10:18315–18322. https://doi.org/10.1039/ d0ra01065k
- Vijayalakshmi S, Kumar E, Ganeshbabu M et al (2021) Structural, electrical, and photocatalytic investigations of PANI/ZnO nanocomposites. Ionics (Kiel) 27:2967–2977. https://doi.org/10.1007/ s11581-021-04041-w
- Aragaw TA, Bogale FM, Aragaw BA (2021) Iron-based nanoparticles in wastewater treatment: a review on synthesis methods, applications, and removal mechanisms. J Saudi Chem Soc 25:101280. https://doi.org/10.1016/J.JSCS.2021.101280
- Dadfar SM, Roemhild K, Drude NI et al (2019) Iron oxide nanoparticles: diagnostic, therapeutic and theranostic applications. Adv Drug Deliv Rev 138:302–325
- Raja K, Mary Jaculine M, Jose M et al (2015) Sol–gel synthesis and characterization of α-Fe2O3 nanoparticles. Superlattices Microstruct 86:306–312. https://doi.org/10.1016/J.SPMI.2015.07.044
- Racik KM, Manikandan A, Mahendiran M et al (2020) Hydrothermal synthesis and characterization studies of α-Fe2O3/MnO2 nanocomposites for energy storage supercapacitor application. Ceram Int 46:6222–6233. https://doi.org/10.1016/j.ceramint.2019.11.091
- Lassoued A, Lassoued MS, Dkhil B et al (2017) Structural, optical and morphological characterization of Cu-doped α-Fe2O3 nanoparticles synthesized through co-precipitation technique. J Mol Struct 1148:276–281. https://doi.org/10.1016/J.MOLSTRUC. 2017.07.051
- Zhang HJ, Meng FN, Liu LZ, Chen YJ (2019) Convenient route for synthesis of alpha-Fe2O3 and sensors for H2S gas. J Alloys Compd 774:1181–1188. https://doi.org/10.1016/J.JALLCOM. 2018.09.384
- Demircioğlu A, Demir KÇ (2021) Effects of annealing on structural, morphological, and corrosion properties of α-Fe2O3 thin films. J Electron Mater 50:2750–2760. https://doi.org/10.1007/s11664-021-08786-y
- Sharma B, Sharma A (2021) Enhanced surface dynamics and magnetic switching of α-Fe2O3 films prepared by laser assisted chemical vapor deposition. Appl Surf Sci 567. https://doi.org/10. 1016/j.apsusc.2021.150724
- Lu Y, Arshad N, Irshad MS et al (2021) Fe2o3 nanoparticles deposited over self-floating facial sponge for facile interfacial seawater solar desalination. Crystals (Basel) 11. https://doi.org/ 10.3390/cryst11121509
- Fouda A, Hassan SED, Abdel-Rahman MA et al (2021) Catalytic degradation of wastewater from the textile and tannery industries by green synthesized hematite (α-Fe2O3) and magnesium oxide (MgO) nanoparticles. Curr Res Biotechnol 3:29–41. https://doi. org/10.1016/j.crbiot.2021.01.004
- Mishra M, Chun DM (2015) α-Fe2O3 as a photocatalytic material: a review. Appl Catal Gen 498:126–141
- Noruozi A, Nezamzadeh-Ejhieh A (2020) Preparation, characterization, and investigation of the catalytic property of α-Fe2O3-ZnO nanoparticles in the photodegradation and mineralization of methylene blue. Chem Phys Lett 752:137587. https://doi.org/10.1016/J.CPLETT.2020.137587
- Bouziani A, Park J, Ozturk A (2020) Synthesis of α-Fe2O3/TiO2 heterogeneous composites by the sol-gel process and their photocatalytic activity. J Photochem Photobiol A Chem 400. https:// doi.org/10.1016/j.jphotochem.2020.112718



Harijan DKL, Gupta S, Ben SK et al (2022) High photocatalytic efficiency of α-Fe2O3 - ZnO composite using solar energy for methylene blue degradation. Physica B Condens Matter 627:413567. https://doi.org/10.1016/J.PHYSB.2021.413567

- Liccardo L, Lushaj E, Dal Compare L et al (2021) Nanoscale ZnO/α-Fe 2 O 3 heterostructures: toward efficient and low-cost photoanodes for water splitting. https://doi.org/10.1002/smsc. 202100104
- Fatima S, Munawar T, Nadeem MS et al (2023) Boosted natural sunlight driven photodegradation of organic dyes using rGO anchored Pr/Cu dual-doped ZnO nanocomposite: characterization and mechanistic insight. Opt Mater (Amst) 136. https://doi.org/10.1016/j.optmat.2022.113397
- Munawar T, Yasmeen S, Hussain F et al (2020) Synthesis of novel heterostructured ZnO-CdO-CuO nanocomposite: characterization and enhanced sunlight driven photocatalytic activity. Mater Chem Phys 249. https://doi.org/10.1016/j.matchemphys.2020.122983
- Goktas S, Goktas A (2021) A comparative study on recent progress in efficient ZnO based nanocomposite and heterojunction photocatalysts: a review. J Alloys Compd 863. https://doi.org/10.1016/j.jallcom.2021.158734
- Ye C, Hu K, Niu Z et al (2019) Controllable synthesis of rhombohedral α-Fe2O3 efficient for photocatalytic degradation of bisphenol A. J Water Process Eng 27:205–210. https://doi.org/10.1016/j. jwpe.2018.12.008
- Nayak SM, Anjum R, Husain J et al (2021) PVA-ZNO nanocomposites thin films for sensing devices. Ferroelectrics 577:221–228. https://doi.org/10.1080/00150193.2021.1916365
- Mukhtar F, Munawar T, Nadeem MS et al (2021) Dual S-scheme heterojunction ZnO–V2O5–WO3 nanocomposite with enhanced photocatalytic and antimicrobial activity. Mater Chem Phys 263. https://doi.org/10.1016/j.matchemphys.2021.124372
- 31. Zulfiqar Ahmed MN, Chandrasekhar KB, Jahagirdar AA et al (2015) Photocatalytic activity of nanocrystalline ZnO, α-Fe2O3 and ZnFe2O4/ZnO. Appl Nanosci (Switzerland) 5:961–968. https://doi.org/10.1007/s13204-014-0395-1
- Handore K, Bhavsar S, Horne A et al (2014) Novel green route of synthesis of ZnO nanoparticles by using natural biodegradable polymer and its application as a catalyst for oxidation of aldehydes. J Macromol Sci, Part A: Pure Appl Chem 51:941–947. https://doi.org/10.1080/10601325.2014.967078
- Peng J, Wang X, Lou T (2020) Preparation of chitosan/gelatin composite foam with ternary solvents of dioxane/acetic acid/water and its water absorption capacity. Polymer Bulletin 77:5227– 5244. https://doi.org/10.1007/s00289-019-03016-2
- Marshall CP, Dufresne WJB, Rufledt CJ (2020) Polarized Raman spectra of hematite and assignment of external modes. J Raman Spectrosc 51:1522–1529. https://doi.org/10.1002/jrs.5824
- 35. Sundara Venkatesh P, Ramakrishnan V, Jeganathan K (2016) Raman silent modes in vertically aligned undoped ZnO nanorods. Physica B Condens Matter 481:204–208. https://doi.org/10.1016/j.physb.2015.11.010
- Silambarasan M, Saravanan S, Soga T (2014) Mn-doped ZnO nanoparticles prepared by solution combustion method. In: e-Journal of Surface Science and Nanotechnology. The Japan Society of Vacuum and Surface Science, pp 283–288
- Jiang J, Oberdörster G, Biswas P (2009) Characterization of size, surface charge, and agglomeration state of nanoparticle dispersions for toxicological studies. J Nanopart Res 11:77–89. https:// doi.org/10.1007/s11051-008-9446-4
- Wang Q, Chen Y, Xu J et al (2018) Morphology-controlled synthesis of Ti-doped α-Fe2O3 nanorod arrays as an efficient photo-anode for photoelectrochemical applications. Res Chem Intermed 44:2365–2378. https://doi.org/10.1007/s11164-017-3234-7
- Venkatesh PS, Purushothaman V, Muthu SE et al (2012) Role of point defects on the enhancement of room temperature

- ferromagnetism in ZnO nanorods. CrystEngComm 14:4713–4718. https://doi.org/10.1039/c2ce25098e
- Saikia L, Bhuyan D, Saikia M et al (2015) Photocatalytic performance of ZnO nanomaterials for self sensitized degradation of malachite green dye under solar light. Appl Catal Gen 490:42–49. https://doi.org/10.1016/j.apcata.2014.10.053
- Diachenko OV, Opanasuyk AS, Kurbatov DI et al (2016) Surface morphology, structural and optical properties of MgO films obtained by spray pyrolysis technique. Acta Phys Pol A 130:805
 810. https://doi.org/10.12693/APhysPolA.130.805
- Norouzzadeh P, Mabhouti K, Golzan MM, Naderali R (2020) Investigation of structural, morphological and optical characteristics of Mn substituted Al-doped ZnO NPs: a Urbach energy and Kramers-Kronig study. Optik (Stuttg) 204. https://doi.org/10.1016/j.ijleo.2020.164227
- Weldegebrieal GK, Sibhatu AK (2021) Photocatalytic activity of biosynthesized α-Fe2O3 nanoparticles for the degradation of methylene blue and methyl orange dyes. Optik (Stuttg) 241. https://doi.org/10.1016/j.ijleo.2021.167226
- 44. Ulfa M, Setiarini I (2022) The effect of zinc oxide supported on gelatin mesoporous silica (GSBA-15) on structural character and their methylene blue photodegradation performance. Bull Chem React Eng Catalysis 17:363–374. https://doi.org/10.9767/bcrec. 17.2.13712.363-374
- Elshypany R, Selim H, Zakaria K et al (2021) Elaboration of Fe3O4/ ZnO nanocomposite with highly performance photocatalytic activity for degradation methylene blue under visible light irradiation. Environ Technol Innov 23. https://doi.org/10.1016/j.eti.2021.101710
- 46. Bibi S, Ahmad A, Anjum MAR et al (2021) Photocatalytic degradation of malachite green and methylene blue over reduced graphene oxide (rGO) based metal oxides (rGO-Fe3O4/TiO2) nanocomposite under UV-visible light irradiation. J Environ Chem Eng 9. https://doi.org/10.1016/j.jece.2021.105580
- Deshmukh SP, Kale DP, Kar S et al (2020) Ultrasound assisted preparation of rGO/TiO2 nanocomposite for effective photocatalytic degradation of methylene blue under sunlight. Nano-Struct Nano-Objects 21. https://doi.org/10.1016/j.nanoso.2019.100407
- Chaudhary K, Shaheen N, Zulfiqar S et al (2020) Binary WO3-ZnO nanostructures supported rGO ternary nanocomposite for visible light driven photocatalytic degradation of methylene blue. Synth Met 269. https://doi.org/10.1016/j.synthmet.2020.116526
- Zeleke MA, Kuo DH (2019) Synthesis and application of V2O5-CeO2 nanocomposite catalyst for enhanced degradation of methylene blue under visible light illumination. Chemosphere 235:935–944. https://doi.org/10.1016/j.chemosphere.2019.06.230
- Mimouni R, Askri B, Larbi T et al (2020) Photocatalytic degradation and photo-generated hydrophilicity of Methylene Blue over ZnO/ ZnCr2O4 nanocomposite under stimulated UV light irradiation. Inorg Chem Commun 115. https://doi.org/10.1016/j.inoche.2020.107889
- 51. Pan D, Ge S, Zhao J et al (2018) Synthesis, characterization and photocatalytic activity of mixed-metal oxides derived from NiCoFe ternary layered double hydroxides. Dalton Trans 47:9765–9778. https://doi.org/10.1039/c8dt01045e
- Pramothkumar A, Senthilkumar N, Jenila RM et al (2021) A study on the electrical, magnetic and optical limiting behaviour of Pure and Cd-Fe co-doped CuO NPs. J Alloys Compd 878. https://doi. org/10.1016/j.jallcom.2021.160332
- Senthilkumar N, Ganapathy M, Arulraj A et al (2018) Two step synthesis of ZnO/Ag and ZnO/Au core/shell nanocomposites: structural, optical and electrical property analysis. J Alloys Compd 750:171–181. https://doi.org/10.1016/j.jallcom.2018.03.348
- Senthilkumar N, Vivek E, Shankar M et al (2018) Synthesis of ZnO nanorods by one step microwave-assisted hydrothermal route for electronic device applications. J Mater Sci Mater Electron 29:2927–2938. https://doi.org/10.1007/s10854-017-8223-5



55. Iqbal T, Irfan M, Ramay SM et al (2020) ZnO–PVA polymer matrix with transition metals oxide nano-fillers for high dielectric mediums. J Polym Environ 28:2422–2432. https://doi.org/10.1007/s10924-020-01768-x

Publisher's Note Springer Nature remains neutral with regard to jurisdictional claims in published maps and institutional affiliations.

Springer Nature or its licensor (e.g. a society or other partner) holds exclusive rights to this article under a publishing agreement with the author(s) or other rightsholder(s); author self-archiving of the accepted manuscript version of this article is solely governed by the terms of such publishing agreement and applicable law.

